AUGUST 27 2003

Drum silencer with shallow cavity filled with helium

Y. S. Choy; Lixi Huang

J. Acoust. Soc. Am. 114, 1477–1486 (2003)
https://doi.org/10.1121/1.1603232

Drum silencer with shallow cavity filled with helium

Y. S. Choy and Lixi Huang[a)]
Department of Mechanical Engineering, The Hong Kong Polytechnic University, Kowloon, Hong Kong

(Received 12 January 2003; revised 6 June 2003; accepted 30 June 2003)

The motivation of this study is twofold: (a) to produce a flow-through silencer with zero pressure loss for pressure-critical applications, and (b) to tackle low frequency noise with limited sideway space using cavities filled with helium. The work represents a further development of our recently conceived device of a drum-like silencer with conventional air cavity [Huang, J. Acoust. Soc. Am. **112**, 2014–2025 (2002); Choy and Huang, *ibid.* **112**, 2026–2035 (2002)]. Theoretical predictions are validated by experimental data. The new silencer consists of two highly tensioned membranes lining part of a duct, and each membrane is backed by a cavity filled with helium. For a typical configuration of a duct with height h, membrane length $L=7h$, cavity depth $h_c=0.2h$, and tension $T=0.52\rho_0 c_0^2 h^2$, where ρ_0 and c_0 are the ambient density and speed of sound in air, respectively, the transmission loss has a continuous stop band of TL$>$6.35 dB for frequency $0.03c_0/h$ to $0.064c_0/h$, which is much better than traditional duct lining. In addition to the mechanisms at work for drum silencers with air cavity, the low density of helium reduces the masslike reactance of the cavity on the second *in vacuo* mode of membrane vibration. The reduction greatly enhances the membrane response at this mode, which is found to be critical for achieving a broadband performance in the low-frequency regime. © *2003 Acoustical Society of America.* [DOI: 10.1121/1.1603232]

PACS numbers: 43.50.Gf, 43.20.Tb, 43.20.Ks [DKW]

I. INTRODUCTION

Low-frequency noise is difficult to control and it still presents a technical challenge. Engineering applications include ventilation systems and flow-through devices such as wind tunnels, engine testing facility, etc. There are two categories of noise control methods: one is passive and another active. Active noise control holds the promise for controlling low-frequency noise, but issues of reliability and cost remain. Passive control is still seen as the ultimate engineering solution. At present, passive control measures mainly rely on duct lining, which is not effective at low frequencies. It also has environmental problems as fibers exposed to flow trap dusts and it could become a health hazard.

Resonators and expansion chambers are the backbone of traditional design of broadband silencer. Different configurations of expansion chambers incorporating resonators have been studied analytically and experimentally. Sullivan (1979a, 1979b) studied, both theoretically and experimentally, the perforated tube muffler formed by one perforated tube enclosed by a chamber. In order to enhance the level of noise reduction and eliminate the passband, further studies on the combination of multiple perforated mufflers were carried out (Thawani and Jayaraman, 1983). There are three main types of multiple perforated tubing mufflers: concentric, plug muffler, and three-duct cross-flow muffler, and their performance are well verified by experiments (Munjal *et al.*, 1993). Mufflers with good performance, such as the plug muffler, tend to carry a penalty of high back pressure. To reduce the pressure drop, a design of two-chamber, three-duct, open-ended muffler is recommended by Gogate and Munjal (1995). It works for a wider frequency range and the pressure drop is not very large. However, it is larger than the concentric and plug type mufflers. As the pressure loss in the muffler connected to an engine or pump wastes power, more power is required for the power source, and this eventually intensifies the noise source. So, apart from the consideration of the environmental aspects and the space occupied, back-pressure is one of the most important attributes of a muffler.

The team led by Fuchs (2001a) has been succeeding in introducing many fiber-free solutions to engineering applications. The key technique is the use of microperforated sheets and other forms of Helmholtz resonators. A device called a membrane absorber box is one such example (Ackermann *et al.*, 1988). Its practical performance as an exhaust stack silencer has been reported by Ackermann and Fuchs (1989). This performance is discussed in some more detail in Sec. IV where comparison is made with the present method.

Recently, Huang (1999) introduced the idea of using tensioned flexible membranes to reflect low-frequency noise. This is a reactive noise control method. The objective is identical to that behind the development of many patented devices by Fuchs and his colleagues (1988, 2001a, 2001b), which is to provide a fiber-free solution. In addition to this, emphasis has been placed on the following two aspects: (a) total noninvasiveness with a view to applications where pressure loss is extremely important or any intrusion into the flow conduit by a muffler is very undesirable, and (b) minimal space required outside the main flow conduit. These objectives are achieved through the use of highly tensioned membranes backed by cavities, and theoretical predictions (Huang, 2002) are validated by experiments (Choy and Huang, 2002). Since the device resembles a drum, it is called a drum-like silencer, or drum silencer henceforth.

The exact mechanisms of a drum silencer have been revealed in detail in Huang (2002) for an idea configuration,

[a)]Author to whom correspondence should be addressed; electronic mail: mmlhuang@polyu.edu.hk

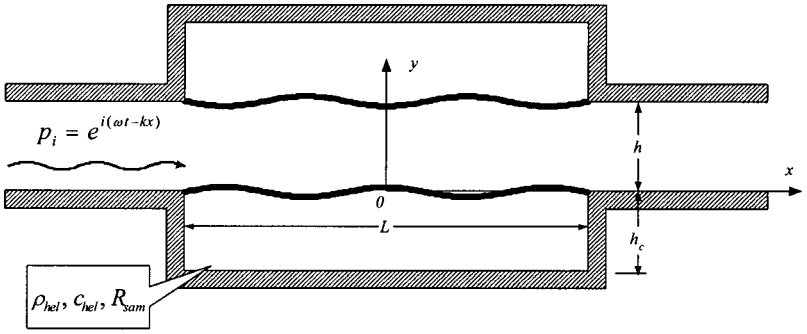

FIG. 1. Configuration model of sound incident on a stretched membrane backed by a cavity filled with helium gas.

and further studies were conducted by Choy (2003) which also takes into account realistic factors such as damping. The findings are now summarized before embarking on the study of helium filled cavities. When the membrane response is decomposed by *in vacuo* modes, it is found that the first two modes play the dominant role. The first mode is most effective in reflecting sound, but it is very difficult to excite due to the relative incompressibility of air inside the cavity. The second mode does not involve any change of cavity volume and is therefore easier to excite, but the radiation efficiency is low due to its dipole-like feature. The third and higher order modes are not very receptive to the incoming low-frequency sound, and they are ineffective in reflecting sound. It is shown that a high tension applied on the membrane promotes the response of the membrane in lower order modes, and the system becomes effective in reflecting sound. The spectra of sound reflection and transmission loss show many peaks at frequencies where sound is almost completely reflected. The performance of the membrane at frequencies between two adjacent peaks can be maintained at a rather high level when appropriate membrane properties are chosen. Damping is not particularly helpful in the enhancement of transmission loss in this case.

The performance of such device is assessed by the level of transmission loss as well as the frequency bandwidth. A rather aggressive criterion of transmission loss is used for the stop band. The lowest frequency which can be controlled in such a drum silencer is typically related to the quarter wavelength of the incident noise, hence related to the length of the membrane. The fundamental reason why long membranes are needed is because the radiation efficiency of the dipole-like second *in vacuo* mode is low for short membranes. This factor is imposed by the sound speed in the main flow duct, which cannot be modified. In order to limit the volume of the cavity, one naturally seeks the reduction of cavity depth. This study explores the use of low density gas like helium in a very shallow cavity, which can be implemented by enclosing the gas in a thin plastic bag, see Sec. III. The result shows that the low acoustic impedance of the gas compensates for the cavity shallowness and the transmission loss achieved is very encouraging. Section II introduces the theoretical prediction method and the optimization of membrane tension. Section III analyzes the results of an optimal configuration found in Sec. II, and Sec. IV compares the theoretical prediction with experimental results.

II. THEORY

Since the details of the basic solution method have been described in Huang (2002) and Choy and Huang (2002), only essential features of the solution and modifications needed for the current study are presented.

A. The solution method

The theoretical model is shown in Fig. 1. The geometry resembles a standard, two-dimensional expansion chamber with a main channel height h, and two identical cavities of length L and depth h_c. Two membranes of length L cover the cavities. With such a cover, the gas medium inside the cavities can differ from air, such as helium gas, and the gas density and speed of sound are denoted as ρ_{hel} and c_{hel} for helium. For convenience, the drum silencer in which the cavity is filled with normal air is denoted as drum-silencer-air, or DSA for short, while that filled with helium as DSH.

Before studying the membrane dynamics, a normalization scheme is introduced to identify controlling parameters. Three basic quantities are used for normalization: the main duct height h as the length scale, air density ρ_0, and the air speed of sound in free space, c_0. The normalized frequencies and the wave number are

$$\bar{f} = fh/c_0, \quad \bar{\omega} = \omega h/c_0 = 2\pi\bar{f}, \quad \bar{k} = kh. \tag{1}$$

The dimensionless first cut-on frequency of the duct is $\bar{f} = 0.5$. The membrane mass per unit area, M, is normalized by $\rho_0 h$, hence the mass ratio $\bar{M} = M/(\rho_0 h)$, and the tensile force T by $\rho_0 c_0^2 h^2$, and pressure by $\rho_0 c_0^2$. For the sake of brevity, all over-bars for dimensionless quantities are dropped henceforth.

When a harmonic sound of unit amplitude $p_i = e^{i(\omega t - k_0 x)}$, where $k_0 = \omega/c_0$ is incident on the membrane, the membrane responds by vibrating at a velocity V, which gives rise to a pressure difference across the two membrane surfaces. If the total loading on the membrane is written as $p_i + \Delta p$, the dynamics of the fluid-structure coupling is described by the following equation for the displacement calculated as $\eta = V/(i\omega)$:

$$M\frac{\partial^2 \eta}{\partial t^2} - T\frac{\partial^2 \eta}{\partial x^2} + \Delta p + p_i = 0. \tag{2}$$

The fluid loading term, Δp, can be divided into three parts. One is the pressure induced on the duct side of the membrane, denoted as $p_{+\mathrm{rad}}$, and the second one is on the cavity

side of the membrane, $p_{-\mathrm{rad}}$, when the cavity is first regarded as an infinite channel of height h_c. The third part, $p_{-\mathrm{ref}}$, is the reflected waves from the two vertical walls in the channel which are actually the end walls of the cavity. $p_{+\mathrm{rad}}$ can be found by the summation over all duct acoustics modes, ψ_m, as shown in the following (Doak, 1973) in dimensional form:

$$p_{+\mathrm{rad}}(x,y,t) = \frac{\rho_0}{2h}\sum_{m=0}^{\infty} c_m\psi_m(y/h)\int_{-L/2}^{+L/2}\psi_m(y'/h)V(x',y',t) \times[H(x-x')e^{-ik_m(x-x')}+H(x'-x)e^{+ik_m(x-x')}]dx', \tag{3}$$

$$\psi_m(y/h)=\sqrt{2-\delta_{0m}}\cos(m\pi y/h), \quad k_m=\frac{\omega}{c_m},$$

$$c_m=\frac{ic_0}{\sqrt{(m\pi/k_0h)^2-1}},$$

where c_m and k_m are the phase speed and wave number of the mth duct mode, respectively, H is the Heaviside function, and δ_{0m} is the Kronecker delta. The integration is carried out over the source surface on $y'=0$, $x'\in[-L/2,L/2]$. To find $p_{-\mathrm{rad}}$ in the lower cavity, ρ_0 and c_0 are replaced by the corresponding properties in the cavity, such as ρ_{hel} and c_{hel} for helium, the vibration velocity V replaced by $-V$, and h replaced by h_c. The reflection loading, $p_{-\mathrm{ref}}$, is found by expressing the standing wave pattern as a sum of duct acoustics expansion like Eq. (3) with two Heaviside functions replaced by two constant, A_m and B_m,

$$p_{-\mathrm{ref}}(x,y,t)=\frac{\rho_{\mathrm{hel}}}{2h_c}\sum_{m=0}^{\infty} c_{mc}\psi_m(y/h_c)\int_{-L/2}^{+L/2}\psi_m(y'/h_c) \times[-V(x',y',t)][A_me^{-ik_{mc}(x-x')} + B_me^{+ik_{mc}(x-x')}]dx', \tag{4}$$

$$c_{mc}=\frac{ic_{\mathrm{hel}}}{\sqrt{(m\pi/k_{\mathrm{hel}}h_c)^2-1}}, \quad k_{\mathrm{hel}}=\frac{\omega}{c_{\mathrm{hel}}}, \quad k_{mc}=\frac{\omega}{c_{mc}},$$

which are found by the rigid wall conditions at $x=\pm L/2$,

$$\left.\frac{\partial(p_{-\mathrm{rad}}+p_{-\mathrm{ref}})}{\partial x}\right|_{x=\pm L/2}=0,$$

$$\rightarrow A_m=\frac{e^{ik_{mc}(L-2x')}+1}{e^{ik_{mc}(2L)}-1},$$

$$B_m=\frac{e^{ik_{mc}(L+2x')}+1}{e^{ik_{mc}(2L)}-1}. \tag{5}$$

The Galerkin procedure is followed to solve Eq. (2). The velocity of the membrane, V, is expanded into a series of sine functions (*in vacuo* modes) for a membrane simply supported at the two edges, $|x|=L/2$,

$$V=\sum_{j=1}^{\infty} V_j\sin j\pi(x/L+1/2),$$

$$V_j=\frac{2}{L}\int_{-L/2}^{+L/2}V(x,t)\sin[j\pi(x/L+1/2)]dx, \tag{6}$$

and the fluid loading is expressed as a sum of modal contributions,

$$\Delta p=\sum_{n=1}^{\infty}\sum_{j=1}^{\infty} V_jZ_{jn}\sin[n\pi(x/L+1/2)], \tag{7}$$

where the single mode impedance Z_{jn} is defined as the nth fluid loading coefficient caused by the vibration of the jth *in vacuo* mode of unit amplitude. The response of the membrane vibration is found by solving the following set of coupled dynamic equations,

$$\mathcal{L}_iV_j+\sum_{n=1}^{N} V_nZ_{jn}=-I_j, \quad j=1,2,..., \tag{8}$$

where

$$I_j=\int_{-L/2}^{+L/2}\frac{2p_i}{L}\sin[j\pi(x/L+1/2)]dx = 2j\pi e^{ik_0L/2}\left[\frac{1-e^{i(-k_0L+j\pi)}}{(j\pi)^2-(k_0L)^2}\right] \tag{9}$$

is the modal coefficient of the incident wave (forcing), and

$$\mathcal{L}_j=Mi\omega-i\frac{T}{\omega}\left(\frac{j\pi}{L}\right)^2 \tag{10}$$

is the *in vacuo* linear operator or membrane reactance. N can be truncated to about 25 and standard matrix inversion techniques like Gaussian elimination can be used. Note that the problem of two membranes shown in Fig. 1 can be solved by splitting the main duct into two parts, each with one membrane and the duct center is replaced by a rigid wall.

Once the vibration velocity is found via the modal coefficient V_j, the reflected wave, denoted as p_r, can be found by evaluating the radiated wave into the far left from Eq. (3), $p_r=p_{+\mathrm{rad}}|_{x\rightarrow-\infty}$, while the transmitted wave, p_t, is found by the superposition of the incident wave, p_i, with the radiation into the far-right, $p_t=p_{+\mathrm{rad}}|_{x\rightarrow+\infty}+p_i$, where $|p_i|=1$. The coefficients of energy flux reflection β, and absorption α, and the transmission loss TL can be evaluated as follows:

$$\beta=|p_r|^2, \quad \alpha=1-\beta-|p_t|^2, \quad \mathrm{TL}=-20\log_{10}|p_t|. \tag{11}$$

The complex amplitude of the reflected sound, p_r, is the sum of contribution made by all individual membrane vibration modes, which is found as follows with the help of Eq. (3):

$$p_r=\frac{1}{2}\int_{-L/2}^{+L/2}V(x')e^{-ik_0x'}dx'=\sum_{j=0}^{\infty}V_jR_j,$$
$$R_j=\frac{1}{2}\int_{-L/2}^{+L/2}\sin[j\pi(x'/L+1/2)]e^{-ik_0x'}dx', \tag{12}$$

where R_j is the complex amplitude of the reflected sound by the induced vibration of the jth mode with unit amplitude.

For the convenience of later analysis, it is pointed out that there is no cross-modal interaction between even and odd modes, and the effects of higher order modes are small at low frequencies (Huang, 2002). As a result, the low-frequency performance can be analyzed in terms of the decomposed first and second mode solutions as

$$V_1=\frac{I_1}{\mathcal{L}_1+Z_{11}},\quad V_2=\frac{I_2}{\mathcal{L}_2+Z_{22}}. \tag{13}$$

B. Prediction of optimal parameters

In a parametric study conducted by Huang (2003), the criterion value of transmission loss to be qualified as stop band is given as follows:

$$\mathrm{TL}_{\mathrm{cr}}=10\log_{10}[1+\tfrac{1}{4}(a_r-a_r^{-1})^2],\quad a_r=1+\sqrt{3\Lambda}, \tag{14}$$

where $\Lambda=2h_cL$ is the total volume of the two cavities. This value is the peak transmission loss of an expansion chamber made of two rectangular cavities which, when put together, form a cubic (square in two dimension) cavity of volume three times the total volume occupied by the drum silencer cavities. The frequency range in which TL satisfies the condition of $\mathrm{TL}\geqslant\mathrm{TL}_{\mathrm{cr}}$ continuously is defined as the stop band, denoted as $[f_1,f_2]$. An optimization procedure is constructed to search for the best tension of the membrane that gives the highest frequency ratio f_2/f_1. In defining the objective function this way, due emphasis is placed on the low frequency noise control. The following set of parameters are used as the default values:

$$M=1.4,\quad h_c=0.2,\quad L=7. \tag{15}$$

The result for the membrane with different tensions and the optimum result are shown in Fig. 2. The performance of the helium filled cavity is compared with that of normal air cavity of the same size. For easier comparison with experimental data, dimensional tension is indicated in Fig. 2 for the test rig of square cross section of $h=100$ mm. Many stop bands are found, but our attention is on the one with the lowest frequency. For the default total volume of the cavity $\Lambda=2h_cL=2.8$, $\mathrm{TL}_{\mathrm{cr}}=6.35$ dB.

When the tension is zero, as shown in Fig. 2(a), there is only inertia effect in the structural property. The spectral pattern is similar to that of a simple expansion chamber when the membrane is removed from the helium cavity. By comparing the frequency ratio f_2/f_1, the dimensional optimum tension to achieve the best performance in the default configuration is found to be 750N with $f_2/f_1=2.17$ as shown in Fig. 2(c). When the tension is lowered to 650N, the TL trough between the first and second peaks in Fig. 2(b) falls below $\mathrm{TL}_{\mathrm{cr}}$. When the tension is increased beyond 750N, the frequency ratio becomes smaller as the first and second peaks close up. f_2/f_1 is about 2.10 for 900N.

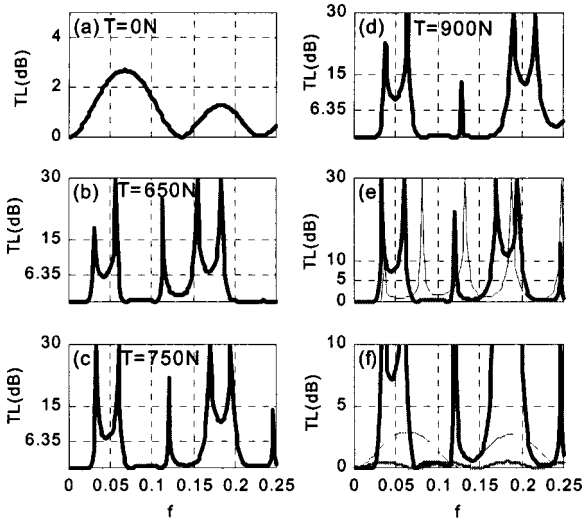

FIG. 2. The prediction of optimal DSH performance and its comparison with other reference configurations. (a), (b), (c), and (d) compare the TL for DSH with membrane tensions of $T=0$N, 650N, 750N(optimal) and 900N; (e) compares the optimal DSH (thick line) with DSA (thin line); (f) compares the optimal DSH (solid line) with expansion chamber with air in the cavity (*), and expansion chamber with helium in the cavity (---).

Having found the optimum tension, 750N, for the membranes backed by helium cavities, more detailed analysis can be carried out. First, comparison is made with the membranes in the air cavity with the same depth (DSA). Figure 2(e) compares the optimal DSH with 750N (thick line), and with DSA with 2870N (thin line). The latter represents the best possible TL pattern for DSA although the best is also mostly below $\mathrm{TL}_{\mathrm{cr}}=6.35$ dB. By now it is apparent that helium cavity can enhance the transmission loss at low frequency. Such performance is attributed to the fluid loading in the cavity and this will be further discussed in the following section. As shown in Fig. 2(f), even when the membrane is removed, the TL of the expansion chamber with helium cavity (---) is much better than that with air cavity (*). The first TL lobe of the helium expansion chamber covers two TL lobes of the air expansion chamber. The width of the lobe is characteristic of a normal expansion chamber with a length of $3.9h$ and the helium expansion chamber also gives much higher TL. This means that the helium cavity is equivalent to a deeper air cavity. Figure 2(f) also compares the DSH (thick line) with the helium expansion chamber, the addition of the membrane is found to enhance the TL level at low frequencies. However, at the very low frequencies ($f<0.027$), DSH degrades the performance of a helium expansion chamber. This will be further explained in the next section.

C. Analysis of the optimal helium filled drum silencer

Focusing on the low-frequency range of $f<0.15$, the spectra of the modal responses for the optimal DSH are shown in Fig. 3. Figure 3(a) shows the TL spectrum in which two peaks and two troughs are marked for membrane response analysis in the right column of Fig. 3. They are $P_1(f=0.0329)$, $P_2(f=0.0587)$, $T_1(f=0.0457)$, and $T_2(f=0.0906)$. Figures 3(b) and (c) analyze the vibration ampli-

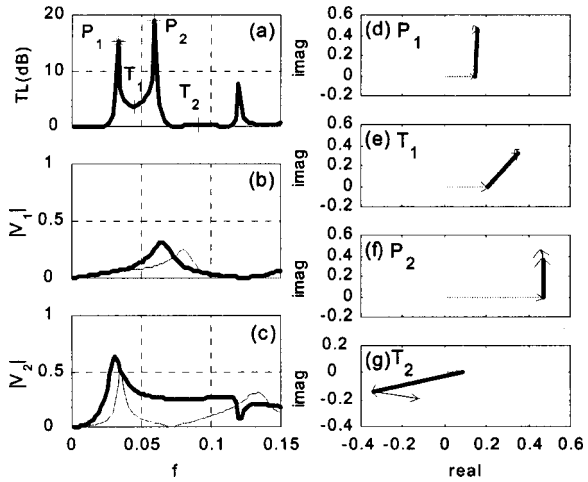

FIG. 3. Modal analysis of the optimal DSH. (a) The TL spectrum of DSH. (b) and (c) Comparison of the modal amplitudes of the first and second order modes of the optimal DSH (thick lines) and those of DSA (thin lines). (d), (e), (f), and (g) The complex modal contributions at the points of P_1, T_1, P_2, and T_2 marked in (a) are plotted.

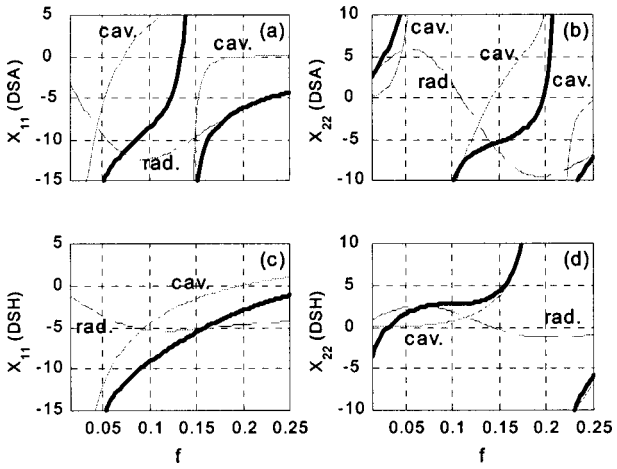

FIG. 4. Reactance of the first two modes of the optimal DSH at $T=750$N and DSA at $T=2870$N. (a) The components of the first mode reactance of DSA. The components are from radiation (marked ''rad''), cavity reflection (marked ''cav''), and the total reactance (thick line) including the structural property. (b) The components of the second mode reactance of DSA. (c) and (d) The first and second mode reactance of the optimal DSH are shown, respectively.

tudes of the first two modes, $|V_{1,2}|$, and compare the results (thick lines) with those of DSA at $T=2870$N (thin lines). In Fig. 3(b), it is observed that the peak of the first modal response of DSH is shifted to lower frequency but the amplitude remains almost identical to that of DSA. In contrast, the second modal response of DSH shown in Fig. 3(c) is greatly increased compared with DSA over a wide frequency range. It is also observed that the second modal response in DSH is higher than the first for the whole frequency range shown in Figs. 3(b) and (c). At about $f=0.065$, the first and second modal responses are almost the same and the levels are not small. This helps to enhance the transmission loss at this particular frequency. To understand the formation of the TL peaks and other frequencies marked in Fig. 3(a), the complex modal reflection contribution (V_jR_j) are shown in the subfigures in the right column as vectors. The first modal reflection (V_1R_1) is taken as the reference direction of real axis, and the second mode is highlighted by thick lines. Figure 3(d) depicts the composition of the modal reflections at the first peak (P_1) of $f=0.0329$. The magnitude of the first modal reflection (V_1R_1) is smaller than the second (V_2R_2). The sum of all the other modes has very small magnitude and it has little effect on the first peak (P_1). Therefore, it can be said that the first TL peak is mainly contributed by the second mode. Figure 3(f) shows the modal reflection contributions for the second peak (P_2) at $f=0.0587$. The first vector is longer than the second, and the two are almost perpendicular to each other, hence no interference. The sum of the rest is again very small, meaning that the higher order modal reflections have almost no effect on the peak. It may be concluded that the second peak P_2 is mainly contributed by the first mode and the second mode is orthogonal to the first.

The point at frequency 0.0436, T_1, lies in between the first and second TL peaks, and is analyzed in Fig. 3(e). In this case, the first and the second modal reflection contributions are almost equally important and there is constructive interference. This is perhaps the reason why the TL dip at this frequency is not too serious. The magnitude of higher order modes is small. The second trough point at $f=0.0906$ is depicted in Fig. 3(g). V_1R_1 is extremely small, while V_2R_2 is relatively large, but it is canceled to a large extent by the sum of other modes. As a result, the transmission loss at this frequency is very small.

The frequency band between the first and second peaks has a desirable transmission loss. This is mainly caused by the dominance of the first and second modes from the above-presented vectorial analysis. The second mode makes larger contributions toward lower frequencies. The spectral variations of responses can be predicted mathematically from Eq. (13), and the analysis should focus on the modal impedance Z_{jn} and structural properties $\mathcal{L}_j$. Figure 4 shows the reactance of the first two modes of the membrane in the air cavity [top row, Figs. 4(a) and (b)], and helium cavity [bottom row, Figs. 4(c) and (d)]. The structural properties for the two cases are different because the optimal tensions are different. The curve marked ''cav'' indicates the cavity reflection effect from $p_{-\mathrm{ref}}$, while the curve marked ''rad'' is for the sum of the radiation from the membrane on the upper and lower sides, $p_{+\mathrm{rad}}+p_{-\mathrm{rad}}$. The thick line represents the total reactance where the structural inertia and stiffness $\mathcal{L}_j$ are also taken into account.

Figures 4(a) and (c) concern the reactance of the first mode for the two configurations. It is observed that the first mode is rather stiff for very low frequencies ($f<0.02$) mainly due to the cavity reflection effect, leading to very weak membrane responses for both DSH and DSA. For the optimal DSA, the cavity stiffness starts to decrease when the frequency goes beyond about 0.02, so the response shown in Fig. 3(a) starts to increase from frequency 0.02 until 0.079. At frequency about 0.144, there is almost no response of the first mode because the reactance diverges at the second cavity mode. This can be seen in Fig. 4(a) in which the total reactance (thick line) tends to infinity at this frequency. For the second modal reactance for DSA in Fig. 4(b), the cavity

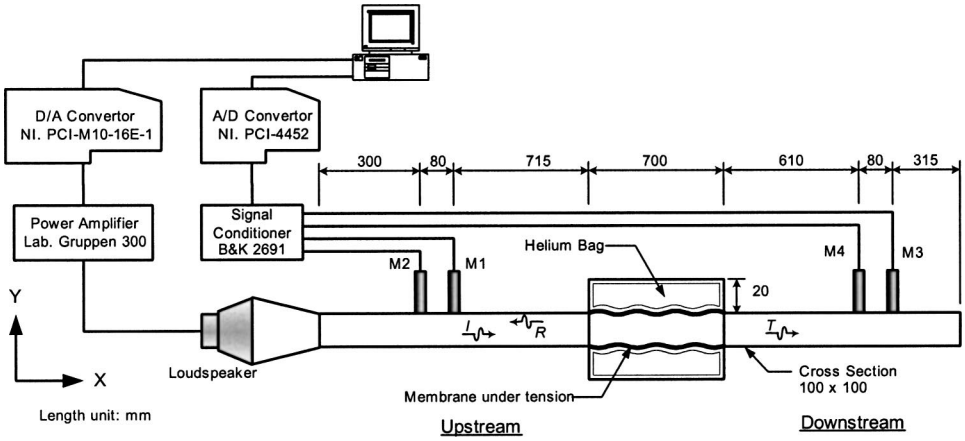

FIG. 5. The setup of the measurement system for DSH using the four-microphone, two-load method. Both data acquisition and the generation of the incident noise are controlled by the computer equipped with A/D and D/A cards, and a LABVIEW code.

modes' divergences occur at two frequencies within the range shown: $f=0.07$, 0.176. Such divergence seriously affects the response of the second mode, and V_2 vanishes at these frequencies. The highly oscillatory patterns of the total reactance shown in Figs. 4(a) and (b) are responsible for the many sharp peaks of TL for DSA in Fig. 2(e).

As shown in Figs. 4(c) and (d), for the optimal DSH, the divergence of the first and second modal reactance basically disappears except at frequency 0.2. It is also observed that the second modal reactance from cavity reflection, and radiation reactance are obviously decreased compared with DSA. The latter is very massive on the second mode for DSA with shallow cavity. The light gas helium effectively relieves the second modal cavity reactance. Therefore, the high response of the second mode can be kept over a wide range of frequency. The dip between the first and second peaks can also maintain a desirable level of TL. Figure 4(d) shows that the total reactance $X_{22}+\mathcal{L}_2$ diverges at frequency 0.2 where $V_2=0$. This represents a big shift from $f=0.07$ for the DSA shown in Fig. 4(b), and the shift provides good performance for low frequencies.

III. EXPERIMENTAL VALIDATION

Theoretical predictions show that the shallow DSH can control the low frequency duct noise by reflection. The stop band lies in the region of very low dimensionless frequencies. As frequency scales by c_0/h, noise of very low dimensional frequencies can be tackled if the cross section of the duct is large. Theoretical predictions like these need to be validated by experiment. Since any experimental rig is three dimensional in nature, the design to simulate the two-dimensional theoretical model should be conducted carefully. The crucial parts of the rig include the tension gear to apply tension uniformly across the third dimension, which is not included in the theoretical model, and the method to measure tension as well as the injection system of the helium gas without leakage from the test rig. The tests give transmission loss, reflection coefficient, and absorption coefficient.

Figure 5 shows the schema of the experimental setup (with dimensions labeled). The duct wall is made of 15-mm-thick acrylic, which is believed to be acoustically rigid. The first cut-on frequency of the duct is 1700 Hz. Two pairs of B&K $\frac{1}{2}$ in. condenser-type, intensity microphones (type number 4187) are installed flush with the duct walls. A wide separation distance of 80 mm is used for the microphone pairs in order to have a good measurement accuracy at low frequencies. The microphones are supported by a B&K's Nexus four-channel conditioning amplifier (type 2691), and the signals are acquired through the National Instruments' AD conversion card type PCI-4452. The noise is generated by a loudspeaker driven by DA signals. Both the AD and the DA processes are controlled by a LABVIEW program, which is made to run through a range of testing frequencies from 20 to 1000 Hz in a loop with a frequency interval of 10 Hz. The output signal from the DA converter (PCI-M10-16E-1) is passed to the loudspeaker via a B&K's power amplifier (LAB Gruppen 300). The discrete frequency approach is preferred. The natural advantage of the pure tone tests is the better signal-to-noise ratio, which is especially important at low frequencies where the loudspeaker is not quite effective. In addition, the sampling rate and sampling period can be adjusted automatically in the LABVIEW code such that an integer number of cycles is guaranteed for all frequencies tested. No digital windowing is needed for the subsequent fast Fourier transform analyses.

The exact locations of the microphones are shown in Fig. 5 with the length unit of mm. The wave components in the upstream side and downstream side indicated in Fig. 5 can be resolved by one pair of microphones on each side. The first test is conducted by putting a rigid plate at the termination of the downstream side. Another set of measurements was taken by replacing the rigid ending plate with a 500-mm-long tube filled with sound absorption materials providing a partially anechoic condition. The linear combination of the intensity fluxes for the two tests then gives a virtual test result in which the downstream is strictly anechoic. This is called the two-load method (Munjal and Doige, 1990). Before doing the experiment, the microphones and the system are calibrated and the procedure can be referred to (Choy, 2001).

In order to keep the helium in the cavity separate from the main duct, a thin plastic membrane bag is used to contain the gas in an air-tight manner. The bag is called, respectively, air bag or helium bag when air or helium is filled into the bag. A cylinder of helium gas with 99% purity produced by a Hong Kong gas company was used. The density and sound speed of helium gas or other gases are obtained from (In-

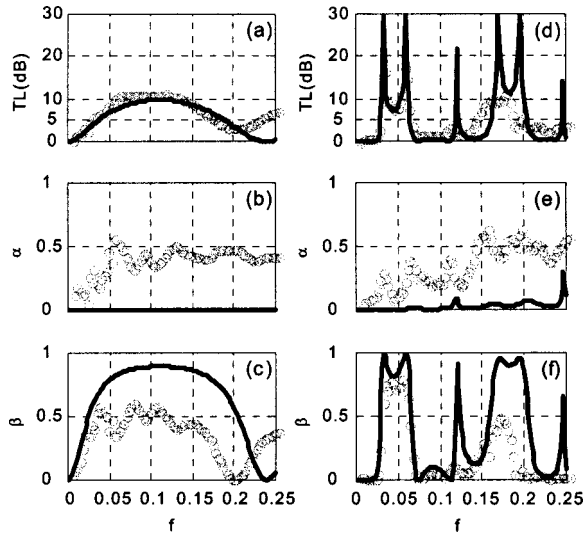

FIG. 6. Comparison of the experimental results (○) with theoretical predictions (—). The left-hand column shows the expansion chamber with helium cavity, but without membrane. The depth and length of the cavity are h and $5h$, respectively. The right-hand column is for the optimal DSH in the default configuration shown in Fig. 5.

cropera and Dewitt, 1996). The two cavities are 20 mm in depth. The plastic bag is made to a rectangular shape to fit into the cavity of 700 mm long and 20 mm deep. The mass per unit area of the plastic is 84 g/m^2.

The membranes are clamped and stretched by a tensile gear, for which the design details are given in Choy (2003) and briefly described here. The upstream end of the membrane is fixed by wrapping it around a cylinder of 12 mm in diameter, while the downstream end of the membrane runs through a 0.1 mm slit, and is fixed by two plates outside the duct. This end can be adjusted easily by the screw which fixes the tension. The tensile force applied is measured by a strain gauge glued to the surface of the membrane in the test section if there is no helium bag.

The stainless steel foil 0.025 mm thick is used in the experiment. The membrane is weighed, and the membrane mass per unit area is 0.17 kg/m^2. The mass ratio is $M/(\rho_0 h)=0.17/(1.225\times 0.1)=1.4$, a value which is used in Eq. (15).

The sub-figures in the left column of Fig. 6 give the experimental results of the helium expansion chamber. There is no metal membrane but the surface of the plastic bag is regarded as the plastic membrane. The dimension of this expansion chamber is not the same as the default values set in Eq. (15). The depth of the cavity of this helium chamber is 100 mm, so the area ratio of the expansion chamber to the duct is 3. The length of the chamber is 500 mm. The open circles represent the experimental result while the solid line is the theoretical prediction. Experimental results of TL in Fig. 6(a) show that the frequency range covered by the first lobe for the helium bag is smaller than prediction. The experimental results can be said to agree quite well with the theory below a frequency of 0.147. In between frequency 0.147 and 0.221, the theory overestimates. Since the maximum TL for a pure expansion chamber of an area ratio of 3 is only 4.4 dB, helium is seen to improve TL and the width of stop band. In Fig. 6(b), the energy loss in the experiment is found to be 45% on average, which takes away the contribution of the reflection coefficient shown in Fig. 6(c). Nevertheless, the main contribution to TL still derives from reflection, and the overall TL pattern in Fig. 6(a) still follows that of β shown in Fig. 6(c) instead of α shown in Fig. 6(b). The reason for the excessive level of α found in experiment is suspected to be the damping of the plastic bag which is under some tension during its inflation by helium. The maximum TL in the experimental result for the helium expansion chamber is found to be 10.6 dB and the peak is not very sharp. The trough goes down to 3 dB instead of 0 dB. The main finding is that both experiments and theory prove that helium can increase the effective depth of the cavity.

The right-hand column in Fig. 6 is for the metal membrane with helium cavity, or DSH, at the optimal condition of $T=750$N. Although there is metal membrane to separate two media in the cavity and the main duct, when the metal membrane is installed, the process of sucking the air out before the injection of helium tends to deform the metal membrane. Therefore, the plastic bag is still employed. Two remarkable peaks are found in the TL spectrum shown in Fig. 6(d). All predicted features are validated by the experimental data shown in open circles, although the peaks found in the experiment are smeared to lower values. The reason for the smearing is revealed by the plot of sound energy absorption coefficient α in Fig. 6(e). The experimental result basically matches the theoretical prediction based on an assumption of material loss factor for stainless steel $\sigma_1=0.5\%$ in the following equation, which is explained in the next section:

$$M(1-i\sigma_1)\frac{\partial^2\eta}{\partial t^2}-T\frac{\partial^2\eta}{\partial x^2}+\Delta p+p_i=0, \tag{16}$$

except at high frequencies ($f>0.147$) where the pattern of experimental data has shifted to lower frequencies. The corresponding stop band is frequency 0.03–0.064 and $f_2/f_1=2.13$ for the experimental results, while the theoretical prediction is 2.16. Notice that the transmission loss between the second and third peaks is very small, a passband, and this band covers a very wide frequency range. The damping of the plastic bag and the friction between the surface of the plastic bag and the rigid wall of the cavity may have caused the deviation between the experiment and theory at higher frequencies beyond the third peak. The absorption energy of the system is about 30% on average and this also causes the pattern of the reflection coefficient to deviate from the theoretical prediction. The main conclusion is that the performance of the DSH with shallow cavity can achieve good performance for the low frequency noise abatement. The energy damping found in helium experiment is further discussed in the following section.

IV. DISCUSSIONS

A. Modeling of the damping mechanism

The experimental data in Fig. 6(b) mean that the energy loss is mainly due to the effect of the plastic bag as there is no metal membrane. The vibration of the plastic bag causes friction with the rigid wall. This results in sound absorption

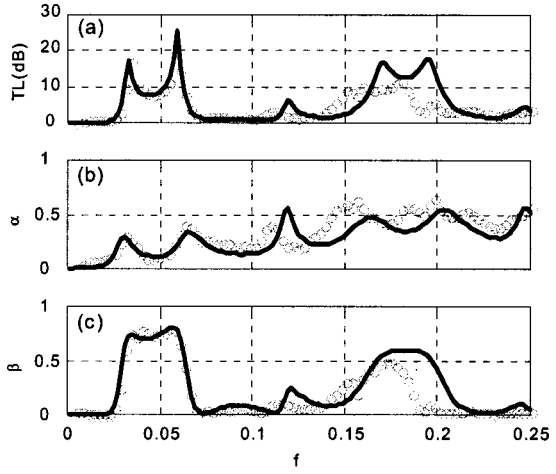

FIG. 7. Comparison of the experimental data (○) with the theoretical damping modeling (—) using $\sigma_1=2\%$, $\sigma_2=2.5\%$, and $R_{\text{sam}}=50\ \text{kg/m}^3\text{s}$.

in the cavity. This effect may be modeled by treating the cavity as one which is filled with some loose sound absorption materials of flow resistivity R_{sam}. This is called the sam-model. In addition, the metal membrane may also cause damping, and this is modeled by attaching damping terms in the following dynamic equation for harmonic oscillations of the fluid loaded membrane;

$$M(1-i\sigma_1)\frac{\partial^2\eta}{\partial t^2}-T(1+i\sigma_2)\frac{\partial^2\eta}{\partial x^2}+\Delta p+p_i=0. \qquad (17)$$

Details of all these damping models are given in Choy and Huang, (2002).

Theoretical tests show that a combination of three damping models with $\sigma_1=2\%$, $\sigma_2=2.5\%$, and $R_{\text{sam}}=50\ \text{kg/m}^3\text{s}$ give the best fit for the experimental data shown in Figs. 6(d), (e), and (f). The result is shown in Fig. 7. When the sam-model is used alone by setting $\sigma_1=\sigma_2=0$, it is difficult to match the first two peaks of α in Fig. 6(e) at $f=0.03$, 0.065. When R_{sam} is too large, it suppresses the first TL peak. The addition of the loss factor in the tensile force term, σ_2, produces better agreement between the theory and experiment for α. It also helps to match all the peaks in TL spectrum in Fig. 7(a). At the high end of the frequencies shown, the energy loss is very large, and this can only be modeled by the loss factor in the inertia term, σ_1. The combination of the three damping models manages to match the experimental results well although there is still some frequency shifting at high frequencies. This deviation may be caused by some uneven curvature of the plastic bag and the absorption in the third direction, which cannot be dealt with by two-dimensional theories.

B. Comparison with other devices

The drum silencer with the shallow helium cavity can help to enhance the noise reduction compared with the shallow air cavity. From the practical point of view, it should be taken to compare with some traditional silencer with the same configuration or dimension. Figure 8(a) shows the comparison of the DSH with duct lining using dimensional frequency as abscissa. The thickness and length of the duct

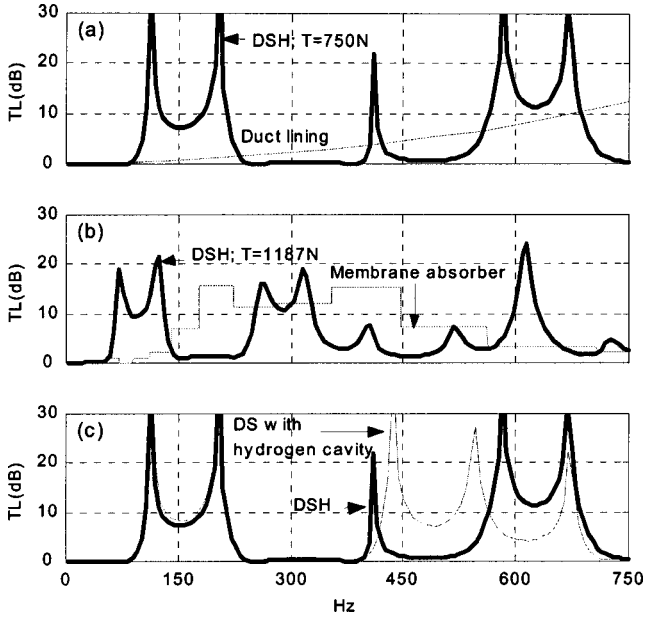

FIG. 8. Comparison between (a) DSH and duct lining, (b) membrane absorber and equivalent DSH, and (c) drum silencers with helium cavity and hydrogen cavity. (a) and (c) are for the default configuration, while (b) is done for the membrane absorber configuration.

lining used are 20 and 700 mm, respectively. The performance of the duct lining is evaluated by the method of Ingard [(1994); p. 6-6, Fig. 6.1.2. with 70% open area and $R=4$]. The DSH is better than the duct lining at low frequencies as such a shallow lining cannot absorb much low frequency noise. The duct lining always causes the hygiene problem to the environment, so the fiber-free DSH is an attractive alternative. However, the DSH performance at the middle frequency range of 200–400 Hz is not desirable.

Figure 8(b) shows the comparison of DSH with the membrane absorber employed as a splitter silencer for which a one-third octave band performance is given in (Ackermann and Fuchs, 1989). The membrane absorber is 1000 mm long and 100 mm wide. The air passage width is 150 mm. Prediction is made for a DSH which is also 1000 mm long and the cavity has a depth of 50 mm on each side of a duct unit of 150 mm in height. Note that a DSH of this dimension may not be the best shape for the given total cavity volume but, nevertheless, the prediction is made for the purpose of simple comparison. As some sound is reflected at the entrance to the splitter and such reflection is not included in the present prediction of DSH performance, the actual sound energy flux entering the splitter region is counted as the true incident wave when the result of Ackermann and Fuchs (1989) is modified for comparison in Fig. 8(b). The contribution of the reflection at the exit of the splitter is not excluded as it is assumed that all reflected sound is absorbed by the membrane absorber. It is observed that the DSH is better than the membrane absorber in the frequency range from 60 to 140 Hz, but, as expected, much worse in the middle passband range.

Figure 8(c) compares the DSH with a drum silencer with cavity filled by hydrogen, which has an even lower density than helium. Predictions are made for the two silencers with the same default geometrical configuration. If there is no

metal membrane covering the hydrogen enclosed by a light plastic bag, the TL peak can be better than that of the helium cavity because the characteristic impedance of hydrogen is even smaller than helium. When the tensioned membranes are added, the optimum tension is found to be 714N. The TL spectrum is generally similar to that of DSH at low frequencies. As helium is chemically more stable than hydrogen, the inert gas of helium is preferred.

C. Practical issues for the use of helium and membranes

Several issues related to the actual implementation of the concept of DSH are discussed here based on what is learnt from the two-dimensional modeling and experiments. The first issue is the significance of the plastic bag. In order to separate two media between the cavity and the main duct, the plastic bag is used, but it should be nonpermeable, and the material should be light enough to allow sound waves to pass through. The second issue is the selection of the material of the metal membrane, which might be exposed to different flow situations. The stress level for the DSH used in this study is around 300 MPa, which falls within the range of fatigue stress of stainless steel, which is around 383 MPa. In order to make sure that no fatigue occurs, good quality material should be chosen. If this DSH is employed in the vehicle exhaust system, the high temperature will cause a vast variation of tension of the metal membrane and this would definitely results in an undesirable performance. The third possible issue is flow-induced vibration. From the extensive studies by Huang (1998, 2001), it seems unlikely that the membrane would experience any form of flutter when the flow speed is well below the *in vacuo* tensile wave speed in the membrane. For the thin stainless membrane used,

$$c_T = \sqrt{\frac{T}{Mh}} = \sqrt{\frac{750}{6860 \times (0.025 \times 10^{-3}) \times 0.1}} = 209.1 \ \text{m/s}.$$

This speed is unlikely to be approached in ordinary ventilation system. However, the problem of self-induced vibration should be more seriously considered if it is used in a high-speed wind tunnel.

V. CONCLUSIONS

The study of full coupling between the sound and membrane with the helium cavity has been carried out through mathematical analysis, physical explanation, and experimental study. The fluid loading by the helium cavity on the membrane and the modal response have been investigated. These help to understand the transmission loss pattern in detail. The following conclusions are drawn for the performance of the DSH with shallow cavities.

(1) Helium provides significant performance enhancement when used in very shallow cavities. With an appropriate tension on the membranes, a very wide stop band can be obtained. This is attributed to the dominance of the first two modes which have higher reflection capability at low frequencies than other higher order modes. The feature of very shallow cavity might be very useful for flow-through silencers with very limited sideway space.

(2) The concept of drum silencer allows the use of different gas in cavities, while a plastic membrane gives the practical realization method to contain the gas.

(3) The use of the light gas liberates the massive fluid loading on the second *in vacuo* mode of the membrane response, while there is little effect on the first order mode. A helium filled cavity is found to increase the response of the second mode substantially, so it helps to increase the noise reduction at low frequencies.

(4) For the typical configuration discussed here, the results represent a viable alternative to duct lining and other fiber-free solutions while maintaining the added advantage of zero backpressure.

(5) The theoretical predictions of the performance of DSH are validated by experimental data despite two major limitations of the theory. One is the two-dimensional nature of the theoretical model, and the other is the lack of knowledge of the damping mechanisms for which only *ad hoc* models are attempted.

(6) Practical issues of DSH have been discussed. It is believed that DSH can be used in the normal air conditioning system, but problems are anticipated in the condition of large temperature variations such as vehicle exhaust.

ACKNOWLEDGMENT

The authors thank the Hong Kong Polytechnic University for its support through various research projects (Nos. G-V618, G-YC 93).

Ackermann, U., and Fuchs, H. V. (**1989**). ''Technical note: Noise reduction in an exhaust stack of a papermill,'' Noise Control Eng. J. **33**, 52–60.

Ackermann, U., Fuchs, H. V., and Rambausek, N. (**1988**). ''Sound absorbers of a novel membrane construction,'' Appl. Acoust. **25**, 197–215.

Choy, Y. S. (**2001**). ''Experimental study of absorption and reflection of grazing sound by flexible panels,'' Proceedings of the Eighth International Congress on Sound Vibrations, Hong Kong, China, 2–6 July, pp. 1003–1010.

Choy, Y. S. (**2003**). ''Sound induced vibration and duct noise control,'' Ph.D. thesis, The Hong Kong Polytechnic University, Hong Kong, China.

Choy, Y. S., and Huang, L. (**2002**). ''Experimental studies of Drum-like silencer,'' J. Acoust. Soc. Am. **112**, 2026–2035.

Doak, P. E. (**1973**). ''Excitation, transmission and radiation of sound from source distribution in hard-walled ducts of finite length. I. The effects of duct cross-section geometry and source distribution space-time pattern,'' J. Sound Vib. **31**, 1–72.

Fuchs, H. V. (**2001a**). ''Alternative fibreless absorbers—new tool and materials for noise control and acoustic comfort,'' Acta Acustica **87**, 414–422.

Fuchs, H. V. (**2001b**). ''Technical and applied papers—From advanced acoustic research to novel silencing procedures and innovative sound treatments,'' Acta Acustica **87**, 407–413.

Fuchs, H. V., Ackermann, U., and Rambausek, N. (**1988**). ''Sound attenuating box,'' United States Patent, US 4 787 473.

Gogate, G. R., and Munjal, M. L. (**1995**). ''Analytical and experimental aeroacoustic studies of open-ended three-duct perforated elements used in muffler,'' J. Acoust. Soc. Am. **97**, 2919–2927.

Huang, L. (**1999**). ''A theoretical study of duct noise control be flexible panels,'' J. Acoust. Soc. Am. **106**, 1801–1809.

Huang, L. (**1998**). ''Reversal of the Bernoulli effect and channel flutter,'' J. Fluids Struct. **12**, 131–151.

Huang, L. (**2001**). ''Viscous flutter of a finite elastic membrane in Poiseuille flow,'' J. Fluids Struct. **15**, 1061–1088.

Huang, L. (**2002**). ''Modal analysis of a Drum-like silencer,'' J. Acoust. Soc. Am. **112**, 2014–2025.

Huang, L. (**2003**). ''Parametric study of a drum-like silencer,'' J. Sound Vib. (unpublished).

Incropera, F. P., and Dewitt, D. P. (**1996**). *Fundamentals of Heat and Mass Transfer* (Wiley, Canada).
Ingard, K. U. (**1994**). *Note on Sound Absorption Technology* (Noise Control Foundation, U.S.A.).
Munjal, M. L., Krishnan, S., and Reddy, M. M. (**1993**). ''Flow-acoustic performance of perforated element mufflers with application to design,'' Noise Control Eng. J. **3**, 159–167.
Munjal, M. L., and Doige, A. G. (**1990**). ''Theory of a two source-location method for direct experimental evaluation of the four-pole parameters of an aeroacoustic system,'' J. Sound. Vib. **141**, 323–333.
Sullivan, J. W. (**1979a**). ''A method for modeling perforated tube muffler components,'' J. Acoust. Soc. Am. **66**, 772–778.
Sullivan, J. W. (**1979b**). ''A method for modeling perforated tube muffler components. II. Application,'' J. Acoust. Soc. Am. **66**, 779–788.
Thawani, P. T., and Jayaraman, K. (**1983**). ''Modeling and application of straight-through resonators,'' J. Acoust. Soc. Am. **73**, 1387–1389.